Polycrystalline iron under compression: Plasticity and phase transitions

Nina Gunkelmann,[1] Eduardo M. Bringa,[2,3] Keonwook Kang,[4] Graeme J. Ackland,[5]
Carlos J. Ruestes,[2] and Herbert M. Urbassek[1,*]

[1]*Physics Department and Research Center OPTIMAS, University Kaiserslautern, Erwin-Schrödinger-Straße, D-67663 Kaiserslautern, Germany*

[2]*Instituto de Ciencias Básicas, Universidad Nacional de Cuyo, Mendoza, 5500 Argentina*

[3]*CONICET, Mendoza, 5500 Argentina*

[4]*Theoretical Division, Los Alamos National Laboratory, Los Alamos, New Mexico 87545, USA*

[5]*School of Physics, The University of Edinburgh, Edinburgh, Scotland*

(Received 16 July 2012; revised manuscript received 24 September 2012; published 16 October 2012)

Iron undergoes a bcc to close-packed structural phase transition under pressure, at around 13 GPa, as shown by diamond anvil and shock experiments. Atomistic simulations have been able to provide insights into the transition, but without any plasticity occurring before the phase change, in single crystals, defective single crystals, or polycrystals. However, experiments in polycrystals do show clear evidence for plasticity. Here we study homogeneous uniaxial compression of polycrystalline Fe using several interatomic potentials: three embedded-atom-model potentials and one modified embedded-atom-model potential. We analyze grain-boundary rotation and dislocation activity, and find that the amount of dislocation activity as a function of strain depends greatly on the potential used. This variation can be explained in terms of the dislocation properties, calculated in this work for each of these potentials.

DOI: 10.1103/PhysRevB.86.144111 PACS number(s): 62.20.F−, 61.72.Lk, 61.50.Ks, 64.70.Nd

I. INTRODUCTION

Iron is one of the crucial components of the universe, and is ubiquitous in the Earth's crust and the Earth's interior. It has clear technological relevance, from the "iron age" till our days, where steels are the structural material of choice in a large variety of settings.

It has been long known that Fe undergoes a structural phase transition at a pressure around 13 GPa, going from body-centered-cubic (bcc) to a hexagonal close-packed (hcp) structure.[1] This phase transition is usually preceded by plastic yielding. For instance, under shock conditions, the experimental signature of plasticity appears as an additional step in the shock wave structure, which for pressures above ∼15 GPa consists of three waves, corresponding to elastic, plastic, and phase changed regions.[2,3]

There was an immense breakthrough in our understanding of this phase transition thanks to the atomistic simulations of Kadau and co-workers,[4–6] and to several dynamic diffraction experiments covering similar time and length scales.[7,8] One outstanding issue remains: current molecular-dynamics (MD) simulations[6] show a phase transition lacking previous dislocation activity in the Fe samples.

There are many atomistic studies of polycrystals under compression. However, most of them deal with face-centered-cubic (fcc) samples.[9] For work on bcc metals, we can mention the papers by Pan *et al.*[10] and Rudd[11] on nanocrystalline (nc) Ta, and Frederiksen *et al.* on nc-Mo,[12] for grain sizes up to ∼20 nm. Farkas and co-workers[13] studied crack propagation in Fe polycrystals and found significant dislocation activity near the crack tip, which indicated the feasibility of observing dislocation-based plasticity in atomistic simulations of polycrystalline Fe under high stress. The effect of grain size on the deformation behavior of nanocrystalline bcc iron under tension was recently studied in MD simulations by Jeon *et al.*,[14] for grain sizes up to nearly 20 nm, and using the potential by Ackland *et al.*[15] They observed a peak in the flow stress averaged over a strain range, as a function of grain size, which was attributed to grain boundary sliding dominating deformation for grain sizes below 10–15 nm, and dislocation activity dominating deformation for larger grains.

In the present paper we use MD simulations to study a nanocrystalline Fe sample, as a model Fe polycrystal. Grain boundaries (GBs) provide dislocation sources, which could be activated to nucleate dislocations under stress. We employ several interatomic potentials, and analyze their dislocation properties. The connection of this study with high pressure experiments is also discussed.

II. SIMULATION METHOD

The public-domain molecular dynamics code LAMMPS[16] was used in this study to perform the simulations.

A. Interaction potentials for iron

Fe belongs to the elements most studied using atomistic simulations, and there are dozens of interaction potentials to simulate different aspects. The pressure-induced transition bcc → close-packed in Fe is closely connected to the magnetic nature of Fe;[17] empirical interatomic interaction potentials nevertheless are able to capture the essential mechanical properties of such phase transitions.

A large fraction of Fe potentials have been created for understanding radiation damage in pressure vessels in nuclear reactors, and focus on reproducing point defect properties at $p = 0$ and relatively low temperatures, below 1000 K. Some potentials aim at describing the melting transition[5,18] and other thermal properties.[19] The Fe pressure-volume relationship is often described by a Rose equation of state,[20] without any consideration for the structural phase transitions, but there is a recent potential developed to reproduce the temperature-

induced close-packed → bcc phase transition at pressures of a few hundred GPa.[21]

A recent review[22] analyzes the ability of several often used Fe potentials to reproduce *ab initio* results, including dislocation core structure, line energy, etc. It was shown that the Mendelev family of potentials[15,22,23] provided a reasonable description of dislocation properties. Those potentials, however, do not describe properly the pressure-induced phase transition bcc to close-packed, since its barrier is assumed high. Here we use the Mendelev potential described in Ref. 23, which can be applied to describe both liquid and solid iron. It is fitted to the first-principles total forces over a liquid atomic configuration.

We also present here a new embedded-atom-model (EAM) potential, similar to the Machová and Ackland potential,[24] but fitted specifically to provide the phase transition. This potential is described in the Appendix and gives a bcc → hcp transition at 13.75 GPa.

The Voter potential[25] has been used extensively to study the bcc → close-packed transition, since it gives a transition pressure close to the experimental value. This includes not only shock-related research,[4,5] but also simulations of single crystals under homogeneous compression.[26] It is fitted to the Rose equation of state and it reproduces well the energetic properties of ferromagnetic bcc iron. This potential typically gives a large fraction of fcc phase, instead of the thermodynamically expected hcp phase. Surprisingly, dislocation properties of the Voter potential have not been studied until now.

Recently, a new modified embedded-atom-model (MEAM) potential was presented for Fe, MEAM-p.[27] It achieves good agreement with the experimental transition pressure paying the price of artificially reducing the energy difference between the phases, compared to *ab initio* results. This issue hinders the goal of achieving a potential offering a realistic comparison to experiments. We note that this MEAM potential also has a phase transition at $p = 0$ and finite T.

For convenience we shall abbreviate the potentials used in the present work as *Voter*,[25] *Mendelev*,[23] *MEAM-p*,[27] and *Ackland* (Appendix of this paper).

B. Sample generation, compression, and analysis methods

Our cubic sample contains approximately 2 million atoms and has an edge length of 30 nm. 64 crystal grains are created in it with random crystallographic orientations using a Voronoi construction method.[28] To equilibrate our systems, we first subjected them to energy minimization using the conjugate gradient method, and then to high-temperature annealing at 80% of their melting temperature during 100 ps. We note that the high-temperature anneal was essential to equilibrate the grain boundaries; the average potential energy per atom decreased from −4.28 to −4.56 eV in the case of the Ackland potential (and similarly for the other potentials) showing the effectiveness of the anneal procedure. Later the samples were cooled back to 10 K. The heating and cooling ramps were performed during 2 ps. Temperature is controlled via velocity scaling. During and after the high-temperature anneal, we used a barostat to keep the pressure at zero. The barostat was anisotropic; it controlled the normal pressures along the three Cartesian directions independently.

We applied periodic boundary conditions to remove any influence of surface effects. Averback and co-workers[29–31] showed that a similar relaxation scheme helps diminishing grain boundary sliding and, therefore, favors dislocation emission. In the simulations, the Verlet integrator is used. Potential cutoffs are defined for each individual potential.

The uniaxial compression along the z axis was carried out at a strain rate of 10^9 s^{-1} and at an initial temperature of 10 K under periodic boundary conditions. We chose this low temperature deliberately as our main aim is to look for plasticity in polycrystalline Fe: since temperature increases under loading, a low starting temperature allows us to identify dislocations relatively easily, as thermal noise is minimal. We performed a number of test simulations at 300 K and found that the higher temperature only increases the noise level without adding new physics.

The samples were deformed up to strains of around 20% during a compression time of 200 ps. During compression we use the NVE ensemble; no temperature control was performed in order to be able to analyze plasticity-driven temperature effects. The samples were visualized using common-neighbor analysis[32,33] and a recently developed technique called the dislocation extraction algorithm (DXA).[34]

III. RESULTS

A. Pressure induced phase transition

Any structural phase transition is driven by the change in Gibbs free energy $G(p,T)$,

$$G = U + pV - TS = H - TS. \quad (1)$$

H is the enthalpy of the system. The phase with lowest G (or lowest H at $T = 0$ K) will be the thermodynamically stable one at a given (p,T).

To measure the transition pressure for the different interatomic potentials we deformed hydrostatically a bcc single crystal with 2000 atoms, as well as the corresponding hcp and fcc structures at $T = 0$ K by rescaling the atomic coordinates. We calculated the enthalpy as a function of pressure, and the intersection of the enthalpies of different phases as a function of pressure gives the transition pressure; see Fig. 1; enthalpies at 10 K are almost identical to those at 0 K.[35] The values of the transition pressures for bcc → hcp and bcc → fcc, together with the energy differences at zero pressures, are listed in Table I. We also include results from *ab initio* calculations and experiment.

MEAM-p and the novel potential presented here are fitted to the phase transition and give results in good agreement with the *ab initio* data. Note, however, the reduced barriers compared to *ab initio* values. The Mendelev potential did not include any fitting of the phase transition and the transition pressure is significantly higher than experiments. The Voter potential was not fitted to the transition, but it gives a reasonably close value.[6]

B. Dislocation properties

In this subsection, using four different interatomic potential models, we investigate properties of a single dislocation in terms of core structure, core energy, and Peierls stress. It is

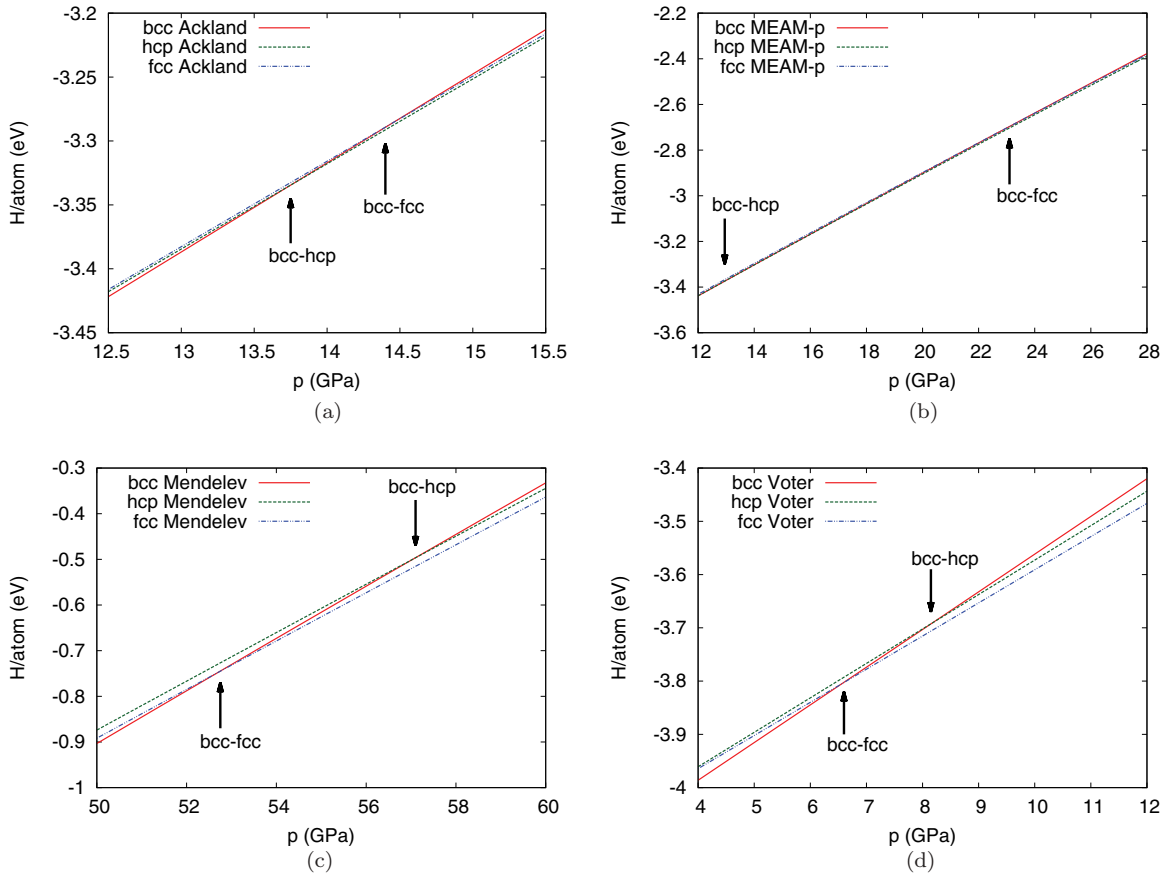

FIG. 1. (Color online) Enthalpies H at 0 K of the bcc, fcc, and hcp structures evaluated for the potentials investigated here. (a) Ackland; (b) MEAM-p; (c) Mendelev; (d) Voter potential. Arrows point at the transition pressures.

generally accepted that the dislocation core structure affects the lattice resistance to dislocation motion and hence crystal plasticity as well.[40] Since the peculiar deformation behaviors in bcc metals are closely related with screw dislocation,[41,42] we confine our focus on the $\langle 111 \rangle/2$ screw dislocation in this work. In order to create dislocation core structures, a screw dipole was constructed using three-dimensional periodic boundary conditions by displacing atoms according to the elasticity solution[43] and then relaxing the position of atoms via the conjugate gradient method. The core energy is calculated as the difference between the atomistic energy of the relaxed structure and the elastic energy of a dipole, later divided by 2 to count the number of dislocations in the cell.[44]

The core structure can have multiple metastable states and the one with lower core energy is the more stable structure. Figures 2 and 3 show differential displacement (DD) maps[45] of the relaxed core structures. Both Ackland and Voter potentials predict a polarized core structure, which asymmetrically dissociates into three {110} planes in two different ways as shown in Figs. 2(a) and 2(b). These two variant structures are geometrically different but energetically identical (cf. core energy in Table II), which is why this type is also called a degenerate core structure. On the other hand, both Mendelev and MEAM-p potentials predict a compact nondegenerate core structure [Fig. 3(a)] and a split-core structure [Fig. 3(b)]. These two structures have different core

TABLE I. Transition pressures and energy differences (at zero pressures) for the potentials investigated. The *ab initio* data are taken from Refs. 6,36–38 and the experimental data from Ref. 39.

Method	$p_{\text{bcc}\to\text{hcp}}$ (GPa)	$p_{\text{bcc}\to\text{fcc}}$ (GPa)	$\Delta E_{\text{bcc-hcp}}(p=0)$ (eV)	$\Delta E_{\text{bcc-fcc}}(p=0)$ (eV)
Ackland	13.75	14.4	0.04	0.04
MEAM-p	12.95	23.1	0.0015	0.008
Mendelev	57.1	52.75	0.12	0.12
Voter	8.1	6.6	0.05	0.01
Ab initio	11.45	19.0	0.07	0.06
Experiment: polycrystal	12.89 ± 0.15			
experiment: monocrystal	14.26 ± 0.14			

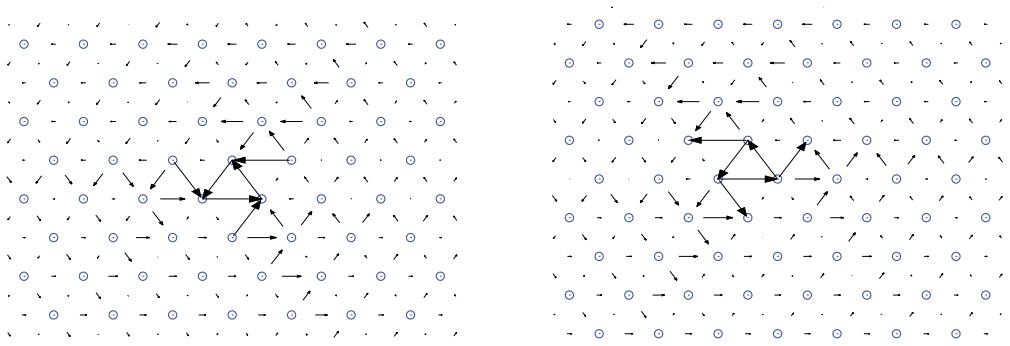

(a) (b)

FIG. 2. (Color online) Ackland and Voter potentials predict degenerate core structures in two variants, (a) and (b).

energies. The nondegenerate core structure has lower core energy in the Mendelev potential, while the split core has lower core energy in the MEAM-p potential.

Another important measure of crystal plasticity is the Peierls stress (τ_P), which is defined as the minimal stress at which a dislocation starts to move at zero temperature. In this work, we externally apply pure shear stress to the simulation cell, which contains a single screw dislocation, along the Burgers vector direction in increments of 100 MPa, until dislocation motion is observed. The Peierls stress as well as the core energy of each potential tested in this work are listed in Table II. What is interesting is that the τ_P of two different core structures are (almost) identical within the same potential, except for the Voter potential. For the Mendelev and MEAM-p potentials, as described in Vitek's study in bcc Mo,[46] the variant core structures become less distinguishable under stress and accordingly the overall behavior of the $\langle 111 \rangle/2$ screw dislocation shows similar response to the applied stress. For degenerate cores, one structure can be more or less mobile than its degenerate one depending on the sense of shearing direction.[47] For the Ackland potential, a less mobile core configuration easily transforms into a mobile one under stress and again the τ_P coincide for the two degenerate core structures. However, in the Voter potential the transformation between the two degenerate cores seems to be very difficult and we see that the τ_P for one configuration is only 3.1 GPa, while for the other configuration the dislocation does not move until the cell collapses at 5.5 GPa. In this case, if the two alternate structures coexist along the dislocation line,[48] the dislocation is most likely to be anchored due to the immobile core configuration.

Overall, the Mendelev potential gives reasonable dislocation properties as mentioned in Ref. 22. The Voter potential does not seem appropriate to describe dislocation-based plasticity in Fe due to its high Peierls stress. MEAM-p seems to give reasonable values but, since the split core configuration is more stable, an initial configuration with a compact core is unstable and transforms into the extended core configuration under shear. The new Ackland potential also shows a degenerate core configuration, with a core polarization which does not agree with *ab initio* calculations.[22]

C. Stress-strain and plastic heating behavior

The von-Mises stress is useful to describe the driving stress for plastic activity. Using the components σ_{ij} of the stress tensor, it is defined as

$$\sigma_{\mathrm{vM}} = \sqrt{\frac{1}{2}\left[(\sigma_{xx}-\sigma_{yy})^2 + (\sigma_{xx}-\sigma_{zz})^2 + (\sigma_{zz}-\sigma_{yy})^2 + 6\left(\sigma_{xy}^2+\sigma_{xz}^2+\sigma_{yz}^2\right)\right]}. \quad (2)$$

Figure 4(a) shows the von-Mises stress versus strain for all simulated potentials.

The stress-strain curves in polycrystals depend on grain-boundary sliding as well as dislocation activity. GB sliding has been shown to be significant mostly for small grains, with grain sizes up to ~15–20 nm.[50–53]

A typical behavior for nanocrystals starts with a narrow linear elastic regime, followed by some GB sliding and then dislocation emission, which lead to a maximum in the von-Mises stress and subsequent plastic relaxation. Because of the presence of plasticity, we cannot pinpoint the phase transition from the stress-strain curves. The plastic relaxation occurs considerably later for the Mendelev potential than for the other potentials; here the high transition pressure prevents the phase transition from starting.

The Voter potential shows significant shear relaxation even at small strains (~3%), when dislocation emission is just starting (see Sec. III D), indicating a large amount of GB sliding (Sec. III F) to relax the applied shear. Dislocation emission in all other potentials, discussed in the next section, starts near the yielding point of the von-Mises stress, and leads to softening of the material.

Figure 4(b) displays the evolution of the diagonal components of the stress tensor with strain. The compression stress

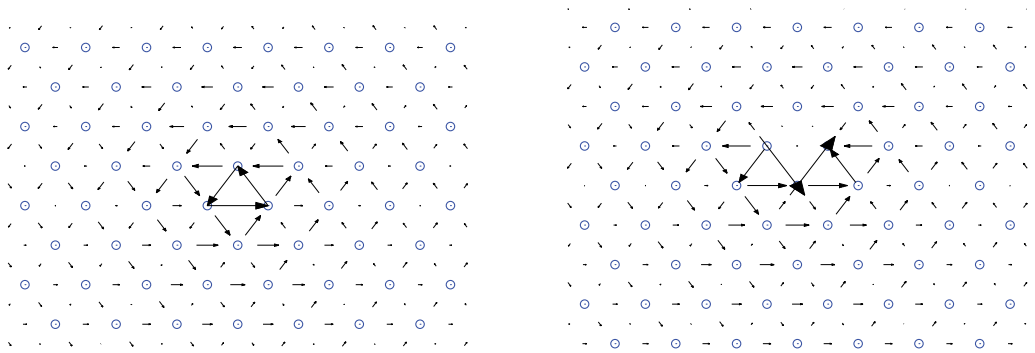

(a) (b)

FIG. 3. (Color online) Mendelev and MEAM-p potentials predict (a) nondegenerate and (b) split-core structures.

for the Voter potential displays an anomalously flat behavior with strain. It features the softness of this potential and is due to GB sliding. Note that all other potentials behave similarly until ∼10% strain. The expected departure at larger strains seen in the Mendelev potential is due to the lack of a phase transformation.

Both GB sliding and dislocation motion lead to plastic heating, seen in Fig. 4(c). However, only the Voter potential displays a huge increase in temperature, indicative of large GB sliding frictional losses, which are consistent with the shear stress relaxation in Fig. 4(a). The unphysically large temperatures reached for the Voter potential will preclude its use in studies including strong plastic effects. Thus the Voter potential gives an example that—even though the phase transition is satisfactorily modeled—the physics of dislocation mobility and in particular GB sliding and rotation has essential impact on the physical reliability of simulation results.

TABLE II. Core structure, core energy, and upper bound for Peierls stress τ_P of a $\langle 111\rangle/2$ screw dislocation. The core energies are given for two values of the cutoff radius, r_c, in the elastic solution for the dislocation energy, and b is the length of the Burgers vector [111]/2. The *ab initio* data are taken from Ref. 49.

Potential	Core type	Core energy E_c (eV/Å)	τ_P (GPa)
Ackland	degenerate 1	0.24853 ($r_c = 2b$)	1.2
		0.32875 ($r_c = 3b$)	
	degenerate 2	0.24843 ($r_c = 2b$)	1.2
		0.32865 ($r_c = 3b$)	
MEAM-p	nondegenerate	0.27955 ($r_c = 2b$)	3.8
		0.35382 ($r_c = 3b$)	
	split-core	0.26875 ($r_c = 2b$)	3.9
		0.34303 ($r_c = 3b$)	
Mendelev	nondegenerate	0.34526 ($r_c = 2b$)	2.9
		0.42554 ($r_c = 3b$)	
	split-core	0.34691 ($r_c = 2b$)	2.9
		0.42719 ($r_c = 3b$)	
Voter	degenerate 1	0.07904 ($r_c = 2b$)	3.1
		0.15926 ($r_c = 3b$)	
	degenerate 2	0.07884 ($r_c = 2b$)	Anchored
		0.15906 ($r_c = 3b$)	
Ab initio			1.3–1.9

D. Dislocation activity

The single dislocation behavior seen in Sec. III B would only provide a rough guide to dislocation activity in a loaded polycrystal. Details of dislocation nucleation at GB have been studied in detail for fcc nanocrystals,[9] but there are few studies for bcc nanocrystals. We display snapshots showing the activation of dislocations and the phase transformation in our nc-Fe crystal in Fig. 5. Note that the CNA analysis employed here was only able to distinguish local bcc environments from non-bcc environments, but could not further analyze the non-bcc environments. Figure 5 allows us to study the changes induced for our nc samples with a complex local stress state; in particular, we observe several nucleation events for dislocations of mixed character, with an edge component running ahead and leaving two straight screw segments on its way to the opposite GB. Sometimes we also observe reactions of dislocations and junction formation.

Snapshots in Fig. 5 show dislocation activity which is quantified in Table III. The Mendelev potential (top row) shows sizable dislocation activity already below ∼12% strain, which in the other potentials is masked by the onset of phase transformation. This activity accompanies the huge von-Mises stress building up for the Mendelev potential [cf. Fig. 4(a)] and is thus due to the unrealistically large transition pressure of this potential. Dislocation nucleation at GBs leads to the softening at larger strains.

All the other potentials investigated, which have their transition pressure at roughly the same (physically correct) value, show roughly comparable behavior. However, the details of the dislocations produced vary from potential to potential, as well as the detailed evolution of the phase transformation, as shown by the frames with a phase transformation at 12%, which are clearly different. In the following, we analyze differences showing up between these potentials, but note that this analysis is at the limit of statistical reliability.

The new Ackland potential only displays reduced dislocation activity, as compared to the Mendelev potential. Note that the von-Mises pressure is almost constant during compression until strains of ∼9%; cf. Fig. 4(a). Thus the material softens here only when the phase transition starts. A detailed analysis reveals that dislocations appear as expected in bcc metals, with several mixed dislocations showing fast edge segments which leave behind straight screw segments.

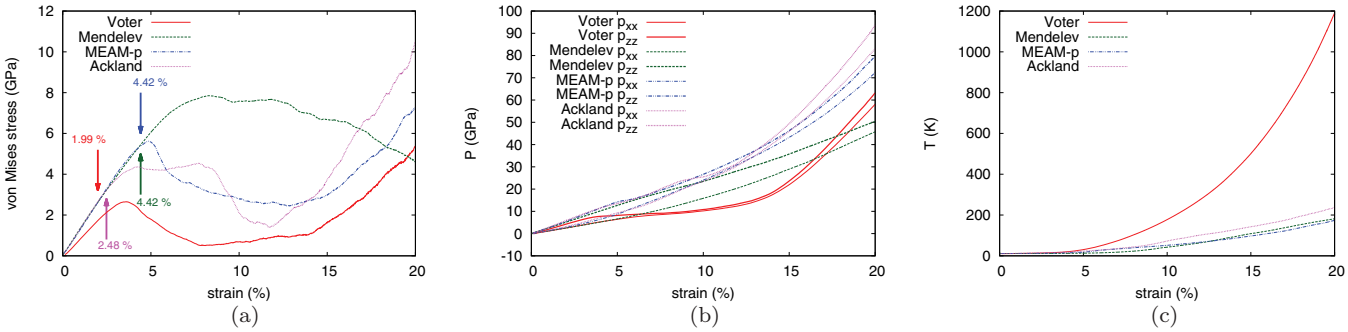

FIG. 4. (Color online) (a) Von-Mises stress, (b) diagonal stress components, and (c) temperature increase versus strain. Arrows in (a) point at the strains where dislocation emission starts.

Before phase transformation, the Voter and Ackland potentials exhibit comparable dislocation densities. Note, however, that the Voter potential showed a strong softening [see Fig. 4(a)] which can be related to the excessive GB sliding; cf. Sec. III F. Because of the highly immobile dislocation configuration of the Voter potential, the comparatively large dislocation density does not lead to observable dislocation-based plasticity, both in our present simulation results and also in earlier shock simulations of polycrystals.[4–6] There is only reduced dislocation activity for MEAM-p, but without large GB rotation seen in Voter, as discussed in Sec. III F.

We have used DXA to analyze dislocations resulting from our uniaxial compression. DXA identifies linear defect structures with a common-neighbor analysis filter, and then can identify those structures with dislocation lines. This procedure works well in single crystals, but in polycrystals the result is less reliable, since DXA can identify some of the initial GBs as dislocation networks. Figure 6 gives an example of the structure of true dislocations evolving during compression of the polycrystal. By an analysis of such snapshots, we observe the first dislocations going from a GB into a grain at von-Mises stresses of 5.45, 3.22, 1.73, and 5.39 GPa for the Mendelev, Ackland, Voter, and MEAM-p potentials, respectively. This means that dislocations do not appear until strains of 4.42%, 2.48%, 1.99%, and 4.42%. Plasticity for lower strains is due to GB sliding for all potentials.

In general, for all nanocrystalline samples, we note that different relaxation schemes will lead to different dislocation densities. For instance, if we generate our polycrystals and perform only energy minimization and a short-term room-temperature annealing without a high-temperature relaxation annealing, there are only a handful of dislocations produced using the Voter potential. However, as noted by Vo *et al.*,[29] this is to be expected, given that the lack of GB relaxation leads to larger GB rotation and reduced dislocation activity. Using high temperature relaxation, there is still a large temperature increase, associated with significant GB rotation, as described in Sec. III F.

E. Phase transformation

At stresses exceeding ∼9% the bcc phase in Fig. 5 becomes increasingly smaller for the Ackland, Voter, and MEAM-p potentials, such that lattice defects (dislocations) can no longer be detected. Instead the material starts phase transforming. We present in Table IV the fraction of material which underwent phase transformation. These results were obtained using the "adaptive CNA" algorithm,[54] which, however, does not provide the local atomic environments. As expected, the Mendelev potential features only a negligible fraction of transformed material, up to the highest compression considered. For the other potentials, the bcc phase has essentially vanished at compressions of around 18%, while the close-packed phases hcp and fcc have built up. Note that the amount of unidentified atoms stays nearly constant during compression. In all potentials that undergo phase transformation, the fraction of hcp is larger than fcc, with the exception of the Voter potential at the highest compression. This is compatible with the nearly degenerate energies of these two close-packed phases.

In order to study the properties of the transformed phase with greater detail—and in particular to decide whether the material will finally transform to hcp or fcc—we "postprocessed" an 8%-compressed specimen (Ackland potential) by hydrostatically compressing it to 100 GPa; at this pressure the specimen has fully phase transformed. Note that due to the kinetics of phase transition an increase of the pressure to values considerably above the transition pressure helps to fully transform the specimen. Due to the application of a hydrostatic—rather than uniaxial—pressure, also the identification of local crystalline order is simplified. Figure 7 demonstrates that the transformation indeed produces hcp-Fe, containing a large number of stacking fault planes. These appear in this plot as fcc material according to their local environment. The stacking faults start and end at grain boundaries and link partial basal dislocations.

F. Grain-boundary rotation

Grain boundary sliding is a process where grain boundaries slip past each other and it was first observed by Adams and Murray in bicrystals of sodium chloride and magnesia.[56] It is driven by rotational or translational strain jumps.[57] It is well known that the total shear stress is influenced by grain boundary sliding and plasticity. Therefore, grain boundary sliding can help suppressing dislocation activity and mobility. On the other hand, it has been shown that high pressures can reduce GB sliding and lead to hardening of nanocrystals.[58] Despite this reduction, simulations by Jarmakani *et al.*[59]

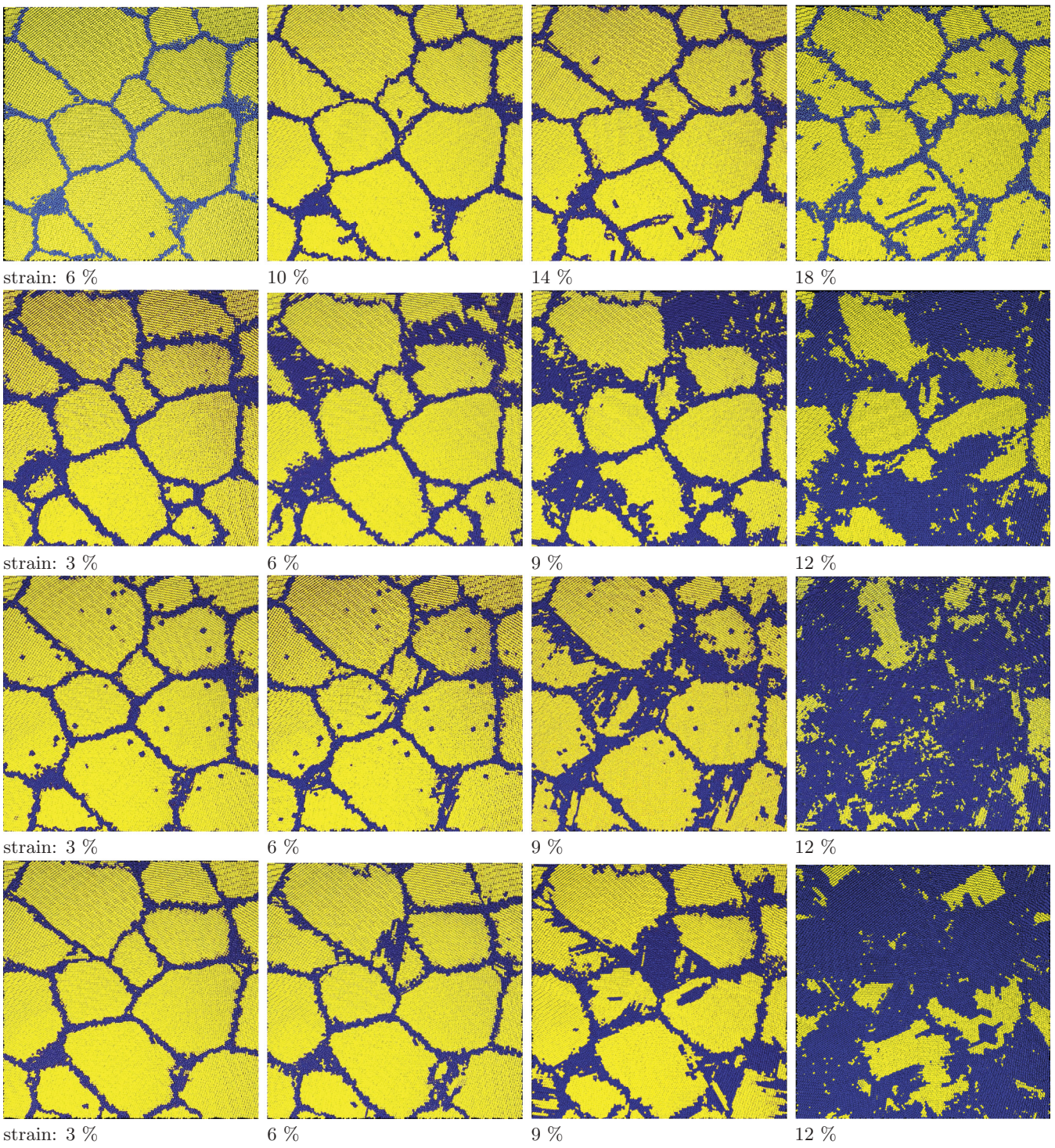

FIG. 5. (Color online) Snapshots showing dislocation activity. System has been cut in a plane perpendicular to the compression direction. Yellow: bcc; blue: other structures, i.e., close-packed structures, grain boundaries, and defects, identified via CNA analysis. The compressive strains increase from left to right from 3% to 6% to 9% to 12%. Only for the Mendelev potential, the strains are higher (6%, 10%, 14%, and 18%). The potentials vary in the row from top to bottom in the sequence: Mendelev, MEAM-p, Ackland, Voter potential.

showed that GB sliding continues to contribute significantly to shock-induced plasticity.

There are several ways to measure GB sliding. Here, to measure the change in grain orientation which indicates grain boundary sliding, we consider two-dimensional cuts on {100} planes. On that plane, we define the local orientation angle θ_i as the angle between the vector connecting atom i to its neighbor and an arbitrary chosen axis (for instance [010]). Using these local angles we can calculate the average grain orientation of the initial sample and compare it to the orientation in a later deformation stage, right before the phase transformation occurs; cf. Fig. 8. The average was estimated by weighting each

TABLE III. Total dislocation density (in 10^{15} m^{-2}) versus strain. The data pertain to the snapshots shown in Fig. 5. Data for the MEAM-p, Ackland, and Voter potentials for 12% strain could not be determined due to the high fraction of phase-transformed material.

	Strain	6%	10%	14%	18%
Mendelev	dislocation density	1.3	3.5	7.4	7.1
	Strain	3%	6%	9%	12%
MEAM-p	dislocation density	0.52	1.1	1.3	
Ackland		0.66	1.7	1.8	
Voter		0.44	1.55	1.21	

average grain orientation with the area of the grain regarding different planes of our polycrystal. We achieve a change in grain orientation for Voter of 2.64°, whereas the average grain rotation for the other three potentials is around 1°. In detail, we observe 0.80°, 1.22°, and 1.20° for the Mendelev, Ackland, and MEAM-p potentials, respectively. These values are lower bounds to GB rotation, since the direction perpendicular to the plane might add an additional rotation angle. We conclude that grain boundary sliding is an important effect for the Voter potential and suppresses dislocation activity.

IV. SUMMARY AND DISCUSSION

We analyzed the response of polycrystalline α-iron to a homogeneous uniaxial compression in order to describe the dislocation activity and the transformation of the initial body-centered cubic phase into a close-packed phase.

Our results show that details of the interatomic interaction potentials, which up to now have only insufficiently been characterized, strongly influence the simulation results. In particular, the Peierls stress, the mobility of dislocations, but also grain rotation and GB sliding essentially influence the phase-change kinetics. It turns out that the often-used Voter potential does not perform well in describing the response of polycrystalline Fe to compression, even though it fairly reproduces the transition pressure: it overestimates GB sliding, leading to material softening and unrealistically large temperature increases during compression under high strain rates. In addition, it predicts a large fraction of fcc phase due to unrealistic bcc → fcc transition pressures.

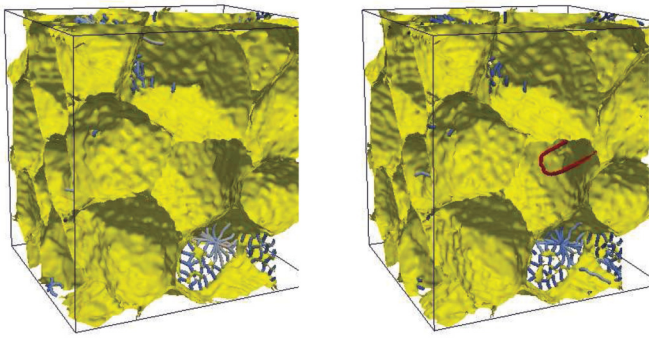

(a) (b)

FIG. 6. (Color online) Snapshots of the sample at (a) 0% and (b) 6% strains, using the Mendelev potential and the DXA tool. Grains are represented as surfaces, with a cut showing the interior of several grains. Dark-blue line segments are GB dislocations, including a spider-web-like dislocation network seen at both 0% and 6% strains, which features a low-angle GB. The red segments at 6% strain represent a dislocation originating at a grain boundary and growing inside a grain.

TABLE IV. Fraction of transformed material for the four potentials (given in %) analyzed with the help of the adaptive CNA algorithm.[54]

Potential	Strain	bcc	hcp	fcc	Disordered
Mendelev	3%	86.09	0.05	0.01	13.85
	6%	85.86	0.05	0.02	14.07
	9%	84.56	0.08	0.08	15.28
	12%	83.27	0.14	0.20	16.39
	15%	81.08	0.31	0.62	17.99
	18%	76.30	1.03	2.73	19.93
MEAM-p	3%	81.13	1.88	1.04	15.94
	6%	65.82	13.30	3.13	17.74
	9%	48.20	27.41	6.11	18.28
	12%	30.03	40.53	10.70	18.75
	15%	8.63	55.37	16.77	19.23
	18%	3.69	55.60	21.68	19.04
Ackland	3%	83.72	0.38	0.25	15.65
	6%	81.79	1.05	0.84	16.32
	9%	57.98	15.87	6.89	19.26
	12%	12.88	49.85	18.41	18.87
	15%	3.59	56.31	22.02	18.08
	18%	1.65	56.28	24.98	17.10
Voter	3%	83.84	0.88	0.48	14.80
	6%	74.10	4.69	4.66	16.55
	9%	55.49	16.30	8.86	19.34
	12%	18.06	45.15	14.70	22.09
	15%	1.28	48.86	29.00	20.86
	18%	0.67	33.33	46.51	19.49

In consequence we investigated the performance of several other Fe potentials. Of these the Mendelev potential shows the best description of dislocations (core energy and configuration, Peierls stress), but displays a significantly too large transition pressure. Two other potentials (the recent MEAM-p and the here presented Ackland potential) possess a realistic transition pressure, but model dislocation properties less accurately.

All potentials used in this study lead to dislocation emission from GBs. Previous studies of shocked polycrystals using the Voter potential did not observe plasticity before the transformation. There are several differences between the simulations presented here and nonequilibrium MD shock simulations, which could account for that. (a) We use homogeneous loading instead of having a compression front, (b) our loading history does not follow a "Hugoniostat,"[60] and (c) the construction and relaxation of nanocrystalline samples might be different and favor GB sliding in the shock simulations.[29–31]

Our analysis of screw dislocations shows that dislocation properties are only described adequately by the Mendelev potential, which yield dislocation densities considerably larger than the other potentials, at strains where the material should have phase changed.

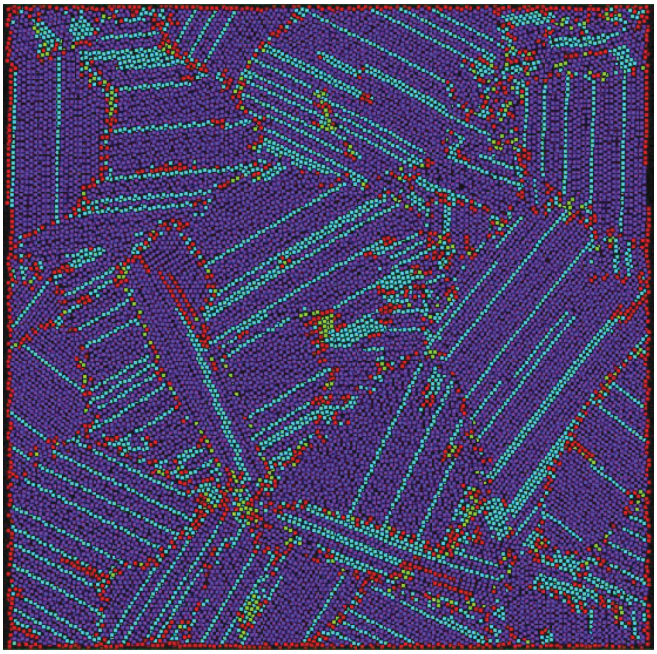

FIG. 7. (Color online) Cross sectional view of the 8%-compressed specimen (Ackland potential) hydrostatically compressed to 100 GPa in order to fully transform the specimen. Local atomic configurations have been analyzed by ballviewer.[55] Dark blue: hcp; light blue: fcc (here: stacking faults); green: bcc (mainly misidentified, but the small region in the center may have survived, screened by the tensile strain field of the surrounding dislocations); red: unidentified (typically grain boundaries). Note that the cross section shown differs from that of Fig. 5.

The new Ackland potential also leads to a correct description of the phase transition pressure. While the dislocation core structures differ significantly from those in the Mendelev potential, dislocation production is sizable.

Using the MEAM-p potential by Lee *et al.*[27] we find the correct phase transformation at 13 GPa, but somewhat reduced dislocation emission. The often used Voter potential yields a phase transition near 10 GPa, but dislocation emission is accompanied by significant GB sliding, as determined by a mean grain reorientation by 2.6°. This correlates well with the large temperature increase during loading.

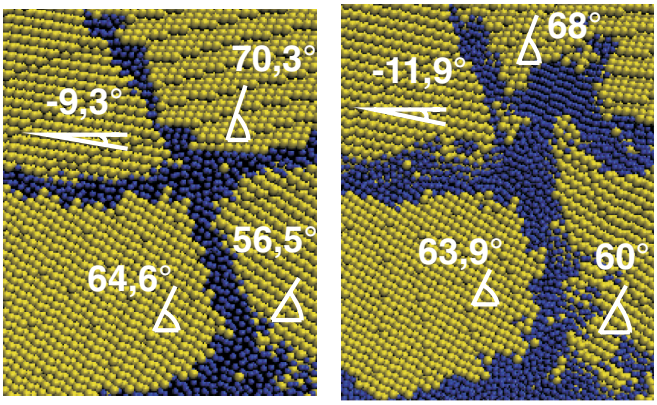

FIG. 8. (Color online) Grain boundary rotation illustrated for compressed crystal (Voter potential). Left: 0% strain; right: 7.1% strain. White lines show local orientation angles in the grains.

Our results are relevant to shock experiments for polycrystalline Fe, indicating that atomistic simulations would be able to display the complex three-wave structure seen in experiments. However, they also point out the complexity of the problem. Even if atomistic simulations are able to describe the phase transition, plasticity details might not be described adequately. In addition, recent experimental results[8] point to a lack of fcc structure, as opposed to a mixture of hcp and bcc phases. The resulting fractions of fcc and hcp close-packed structures would also depend on details of the potentials, with Voter predicting mostly an fcc phase.

Details of the phase transition will depend not only on the free-energy barriers, but also on the resulting kinetics.[61] Phase stability might also be affected by the nanoscale structure of the samples.[62]

Fe shock experiments have dealt so far with large grains, with a typical size of 1–100 μm. For such samples, plasticity at high pressures is likely related to the activation of dislocation sources inside grains, with a minor contribution from GB sources. Such sources would typically have a much lower activation stress than GB sources, and would then lead to much lower elastic limits. However, high-strain-rate effects also lead to an increase of the yield stress, and the values we obtain here, of a few GPa, are not far from the results of Smith *et al.*[3]

We note that compression-induced shear in our simulated nanograins might lead to lowering of the transition pressure, as predicted by models[63] and experiments.[64] Furthermore, plasticity occurs in our sample only by grain-boundary motion and by grain-boundary nucleation of a few dislocations. The volume inside our grains is initially dislocation-free, and the size of our grains precludes the formation of pileups, which might in turn help nucleating the new phase or further dislocation activity, as proposed in Ref. 65.

The issue of defect nucleation during plastic flow is of general interest. In our samples, plastic flow is caused by the nucleation of relatively few dislocations from grain boundaries. Nucleation of dislocations from GBs has been studied in detail for a number of nanocrystals,[66] and it has been found to depend heavily on the orientation of grains separated by the GB, on GB structure, on the local stress state, etc. In our study, we use polycrystals which are large enough to contain a large collection of GBs and, therefore, are able to give a reasonable "average" plastic deformation.

Future simulations will cover nonequilibrium MD shock simulations of nanocrystals using various potentials, and also recovery of loaded samples. Given the high Peierls barriers for dislocation motion in bcc metals, the amount of recovery would be significantly less than in fcc samples and, therefore, recovery experiments might be directly comparable to MD results including unloading and relaxation.

Finally, future experiments using nc-Fe samples are now feasible and would allow a direct comparison between MD simulations and experiments at similar time and length scales.

ACKNOWLEDGMENTS

This work has been supported by the *Deutsche Forschungsgemeinschaft* via the Sonderforschungsbereich 926. E.M.B.

TABLE V. Parameters for the new potential, Eqs. (A3) and (A4), in units of eV and iron lattice parameter ($a_0 = 2.866$ Å).

a_k (eV/a_0^3)	− 31.807065	36.158663	12.237970	− 72.863506	156.864024	200.148093
A_k (eV^2/a_0^3)	72.868383	− 100.944857				
r_k (a_0)	1.450000	1.430000	1.080000	0.990000	0.930000	0.866025
R_k (a_0)	1.300000	1.200000				

acknowledges support from CONICET, SeCTyP (U. N. Cuyo), and PICT-2009-0092. K.K. acknowledges support from the Leading Foreign Research Institute Recruitment Program through the National Research Foundation of Korea funded by the Ministry of Education, Science and Technology (2011-0030065).

APPENDIX: NEW POTENTIAL

The new potential is a simple amendment to a previous Finnis-Sinclair potential from 1997.[67] That potential was fitted to the lattice parameter 2.866 Å, elastic constants $C_{11} = 243$, $C_{12} = 145$, and $C_{44} = 116$ GPa, cohesive energy 4.316 eV, and unrelaxed vacancy formation energy 1.79 eV. It stabilizes the bcc structure, and has an α-ϵ phase transition, but at too high a pressure. Other potentials examined here[23,25,27] generally have an α-ϵ transition at pressure. Although it would be desirable to have all phases ($\alpha, \gamma, \delta, \epsilon$) stable, and include the effect that γ is stabilized in potentials for steel by small amounts of carbon,[68] we were unable to easily convert other existing potentials to have the correct α-ϵ transition. Consequently, we refitted the high-pressure behavior of the 1997 potential to obtain an α-ϵ transition pressure at 13.75 GPa. The refitting was done by adjusting the short-range part of the potential, which has the side effect of raising the melting point to 2700 K; however, we do not approach the melting temperature in this work.

The energy is written as

$$\mathcal{U} = \sum_i F(\rho_i) + \frac{1}{2}\sum_{i,j\neq i} V_{ij}(r_{ij}), \tag{A1}$$

with

$$\rho_i = \sum_{j\neq i} \phi_{ij}(r_{ij}). \tag{A2}$$

The functions ϕ and V were defined as cubic splines; F is given by its Finnis-Sinclair form ($F = \rho^{1/2}$) and

$$V(r) = \sum_{k=1}^{6} a_k (r_k - r)^3 H(r_k - r), \tag{A3}$$

$$\phi(r) = \sum_{k=1}^{2} A_k (R_k - r)^3 H(R_k - r), \tag{A4}$$

where $H(x)$ is the Heaviside step function: $H(x) = 0$ for $x < 0$ and $H(x) = 1$ for $x > 0$. The various parameters are given in Table V.

*urbassek@rhrk.uni-kl.de; http://www.physik.uni-kl.de/urbassek/

[1] W. Pepperhoff and M. Acet, *Constitution and Magnetism of Iron and its Alloys* (Springer, Berlin, 2001).
[2] J. C. Boettger and D. C. Wallace, Phys. Rev. B **55**, 2840 (1997).
[3] R. F. Smith, J. H. Eggert, R. E. Rudd, D. C. Swift, C. A. Bolme, and G. W. Collins, J. Appl. Phys. **110**, 123515 (2011).
[4] K. Kadau, T. C. Germann, P. S. Lomdahl, and B. L. Holian, Science **296**, 1681 (2002).
[5] K. Kadau, T. C. Germann, P. S. Lomdahl, and B. L. Holian, Phys. Rev. B **72**, 064120 (2005).
[6] K. Kadau, T. C. Germann, P. S. Lomdahl, R. C. Albers, J. S. Wark, A. Higginbotham, and B. L. Holian, Phys. Rev. Lett. **98**, 135701 (2007).
[7] D. H. Kalantar, J. F. Belak, G. W. Collins, J. D. Colvin, H. M. Davies, J. H. Eggert, T. C. Germann, J. Hawreliak, B. L. Holian, K. Kadau *et al.*, Phys. Rev. Lett. **95**, 075502 (2005).
[8] J. A. Hawreliak, B. El-Dasher, H. Lorenzana, G. Kimminau, A. Higginbotham, B. Nagler, S. M. Vinko, W. J. Murphy, T. Whitcher, J. S. Wark *et al.*, Phys. Rev. B **83**, 144114 (2011).
[9] M. A. Meyers, A. Mishra, and D. J. Benson, Prog. Mater. Sci. **51**, 427 (2006).
[10] Z. L. Pan, Y. H. Li, and Q. Wei, Acta Mater. **56**, 3470 (2008).
[11] R. E. Rudd, Mater. Sci. Forum **633-634**, 3 (2009).
[12] S. L. Frederiksen, K. W. Jacobsen, and J. Schiøtz, Acta Mater. **52**, 5019 (2004).
[13] A. Latapie and D. Farkas, Model. Simul. Mater. Sci. Eng. **11**, 745 (2003).
[14] J. B. Jeon, B.-J. Lee, and Y. W. Chang, Scr. Mater. **64**, 494 (2011).
[15] G. J. Ackland, M. I. Mendelev, D. J. Srolovitz, S. Han, and A. V. Barashev, J. Phys.: Condens. Matter **16**, S2629 (2004).
[16] http://lammps.sandia.gov/
[17] M. Ekman, B. Sadigh, K. Einarsdotter, and P. Blaha, Phys. Rev. B **58**, 5296 (1998).
[18] A. B. Belonoshko, R. Ahuja, and B. Johansson, Phys. Rev. Lett. **84**, 3638 (2000).
[19] M. Müller, P. Erhart, and K. Albe, J. Phys.: Condens. Matter **19**, 326220 (2007).
[20] J. H. Rose, J. R. Smith, F. Guinea, and J. Ferrante, Phys. Rev. B **29**, 2963 (1984).
[21] A. B. Belonoshko, P. M. Derlet, A. S. Mikhaylushkin, S. I. Simak, O. Hellman, L. Burakovsky, D. C. Swift, and B. Johansson, New J. Phys. **11**, 093039 (2009).
[22] L. Malerba, M. C. Marinica, N. Anento, C. Björkas, H. Nguyen, C. Domain, F. Djurabekova, P. Olsson, K. Nordlund, A. Serra *et al.*, J. Nucl. Mater. **406**, 19 (2010).
[23] M. I. Mendelev, S. Han, D. J. Srolovitz, G. J. Ackland, D. Y. Sun, and M. Asta, Philos. Mag. **83**, 3977 (2003).
[24] A. Machová and G. J. Ackland, Model. Simul. Mater. Sci. Eng. **6**, 521 (1998).

[25]R. J. Harrison, A. F. Voter, and S.-P. Chen, in *Atomistic Simulation of Materials: Beyond Pair Potentials*, edited by V. Vitek and D. J. Srolovitz (Plenum Press, New York, 1989), p. 219.
[26]B. T. Wang, J. L. Shao, G. C. Zhang, W. D. Li, and P. Zhang, J. Phys.: Condens. Matter **22**, 435404 (2010).
[27]T. Lee, M. I. Baskes, S. M. Valone, and J. D. Doll, J. Phys.: Condens. Matter **24**, 225404 (2012).
[28]A. Frøseth, H. Van Swygenhoven, and P. Derlet, Acta Mater. **53**, 4847 (2005).
[29]N. Q. Vo, R. S. Averback, P. Bellon, S. Odunuga, and A. Caro, Phys. Rev. B **77**, 134108 (2008).
[30]N. Q. Vo, R. S. Averback, P. Bellon, and A. Caro, Phys. Rev. B **78**, 241402 (2008).
[31]N. Q. Vo, R. S. Averback, P. Bellon, and A. Caro, Scr. Mater. **61**, 76 (2009).
[32]D. Faken and H. Jonsson, Comput. Mater. Sci. **2**, 279 (1994).
[33]H. Tsuzuki, P. S. Branicio, and J. P. Rino, Comput. Phys. Commun. **177**, 518 (2007).
[34]A. Stukowski and K. Albe, Model. Simul. Mater. Sci. Eng. **18**, 085001 (2010).
[35]C. Engin, L. Sandoval, and H. M. Urbassek, Model. Simul. Mater. Sci. Eng. **16**, 035005 (2008).
[36]H. C. Herper, E. Hoffmann, and P. Entel, Phys. Rev. B **60**, 3839 (1999).
[37]Q. Chen and B. Sundman, J. Phase Equil. **22**, 631 (2001).
[38]Z.-Y. Zeng, C.-E. Hu, X.-R. Chen, L.-C. Cai, and F.-Q. Jing, J. Phys.: Condens. Matter **20**, 425217 (2008).
[39]B. J. Jensen, G. T. Gray III, and R. S. Hixson, J. Appl. Phys. **105**, 103502 (2009).
[40]W. Cai, V. V. Bulatov, J. Chang, J. Li, and S. Yip, in *Dislocations in Solids*, edited by F. R. N. Nabarro and J. P. Hirth (North-Holland, Amsterdam, 2004), Vol. 12, p. 1.
[41]M. S. Duesbery, in *Dislocations in Solids*, edited by J. P. Hirth and L. Kubin (Elsevier, Amsterdam, 1989), Vol. 8, p. 67.
[42]M. S. Duesbery and V. Vitek, Acta Mater. **46**, 1481 (1998).
[43]W. Cai, V. V. Bulatov, J. Chang, J. Li, and S. Yip, Philos. Mag. **83**, 539 (2003).
[44]V. V. Bulatov and W. Cai, *Computer Simulations of Dislocations* (Oxford University Press, Oxford, 2006), Chap. 5.2.
[45]V. Vítek, R. C. Perrin, and D. K. Bowen, Philos. Mag. **21**, 1049 (1970).
[46]V. Vítek, Philos. Mag. **84**, 415 (2004).
[47]K. Ito and V. Vítek, Philos. Mag. A **81**, 1387 (2001).
[48]F. Kroupa, Phys. Status Solidi **3**, K391 (1963).
[49]D. Caillard, Acta Mater. **58**, 3504 (2010).
[50]J. Schiotz, T. Vegge, F. D. Di Tolla, and K. W. Jacobsen, Phys. Rev. B **60**, 11971 (1999).
[51]H.-H. Fu, D. J. Benson, and M. A. Meyers, Acta Mater. **49**, 2567 (2001).
[52]K. W. Jacobsen and J. Schiotz, Nat. Mater. **1**, 15 (2002).
[53]H. Van Swygenhoven, Science **296**, 66 (2002).
[54]A. Stukowski, Model. Simul. Mater. Sci. Eng. **20**, 045021 (2012).
[55]G. J. Ackland and A. P. Jones, Phys. Rev. B **73**, 054104 (2006).
[56]M. A. Adams and G. T. Murray, J. Appl. Phys. **33**, 2126 (1962).
[57]J.-H. Ree, J. Struct. Geol. **16**, 403 (1994).
[58]E. M. Bringa, A. Caro, Y. Wang, M. Victoria, J. M. McNaney, B. A. Remington, R. F. Smith, B. R. Torralva, and H. Van Swygenhoven, Science **309**, 1838 (2005).
[59]H. N. Jarmakani, E. M. Bringa, P. Erhart, B. A. Remington, Y. M. Wang, N. Q. Vo, and M. A. Meyers, Acta Mater. **56**, 5584 (2008).
[60]J.-B. Maillet, M. Mareschal, L. Soulard, R. Ravelo, P. S. Lomdahl, T. C. Germann, and B. L. Holian, Phys. Rev. E **63**, 016121 (2000).
[61]L. T. Kong, J. F. Li, Q. W. Shi, H. J. Huang, and K. Zhao, Europhys. Lett. **97**, 56004 (2012).
[62]Q. Meng, Y. Rong, and T. Y. Hsu, Phys. Rev. B **65**, 174118 (2002).
[63]K. J. Caspersen, A. Lew, M. Ortiz, and E. A. Carter, Phys. Rev. Lett. **93**, 115501 (2004).
[64]Y. Ma, E. Selvi, V. I. Levitas, and J. Hashemi, J. Phys.: Condens. Matter **18**, S1075 (2006).
[65]V. I. Levitas, Phys. Rev. B **70**, 184118 (2004).
[66]K. S. Kumar, H. Van Swygenhoven, and S. Suresh, Acta Mater. **51**, 5743 (2003).
[67]G. J. Ackland, D. J. Bacon, A. F. Calder, and T. Harry, Philos. Mag. A **75**, 713 (1997).
[68]D. J. Hepburn and G. J. Ackland, Phys. Rev. B **78**, 165115 (2008).